

Macroscopic Elastic Constitutive Relationship of Cast-in-Place Hollow-Core Slabs

Jing-Zhong Xie¹

Abstract: The macroscopic Poisson ratio and elastic moduli of the cast-in-place hollow-core slab are researched in this paper. At first, the formulas for computing the Poisson's ratio of cast-in-place hollowed slabs with bilateral ribs are deduced by theoretical means. Then, based on the characteristics of stress distribution, an effective sectional area method is proposed for computing both the bending and axial compressive elastic moduli of cylindrical hollow-core slabs at the transverse section, in which the boundary of the effective area is suggested to be at a radial distance with its vertical slope angle $\alpha_0=22.5^\circ$. Relevant formulas for computational purposes are also proposed. At last, the shear modulus of cylindrical hollow-core slab at the transverse section is proposed to be computed considering the bending-shear deformation of the varying rib and face sheets at a periodic segment, and relevant formulas for curved sides beam are also deduced. In the course of the study, the so-called transverse-rib-effect phenomenon in which the transverse rib of hollow-core slab may lead to macroscopic stiffness increase has been revealed, which is modeled by an appropriate mathematical relationship. The proposed methods and formulas are carefully evaluated analytically and numerically and may be the foundations for structural analysis of cast-in-place hollow-core slabs.

DOI: 10.1061/(ASCE)0733-9445(2009)135:9(1040)

CE Database subject headings: Concrete slabs; Hollow sections; Constitutive relations; Anisotropy; Poisson ratio; Shear modulus; Elasticity.

Introduction

The cast-in-place hollow-core slab in which the inner mold left in place is being popularly used in China recently. The shapes of inner mold are usually cylindrical tube or cubic box, which are denoted as cylindrical hollow-core slab and cubic hollow-core slab as shown respectively in Figs. 1 and 2. The inner molds are mainly formed with precast concrete, precast fiber reinforced concrete, foam, or thin-walled steel tube.

This hollow-core slab can be used for beam-and-slab floor, but mainly for flat-slab floor structures. The usual constitution of this kind of slab-column structure is shown in Fig. 3. There are three parts in the floor, the solid zone around the column, the solid strip between the columns, and the hollow-core slab for the rest of the floor. The solid zone is usually made thicker than the strip and the hollow-core slab to resist concentrated bending moment and to improve punching capability. The real construction of this slab can be seen in Fig. 4.

The excellent mechanical property of the hollow-core slab contributes to the superiority of the flat-slab floor structures by simplifying reinforcing bar placement and mold shaping which then reduces construction time. It also decreases the total weight and height of the building. Due to a number of previous applications and findings from several research projects, load-capacity

criteria are now listed in the China Design Code CECS: 175-2004 [China Association for Engineering Construction Standardization (CECS) 2004].

A similar cast-in-place hollow-core slab (BubbleDeck slab) can be found in the literature. For this type of slab, the inner mold consists of a small plastic ball. The punching behavior of a slab without a similar solid zone around the joint (as shown in Fig. 3) was researched by Schnellenbach-Held and Pfeffer (2002). Relevant findings from their work are included in the German design code DIN 1045. Chinese literature reports, Huang et al. (1997), introduced the application of a new style hollow-core slab, and Lou et al. (2005) reported the internal forces distribution and slab displacements in a full scale experiment. The honeycomb-core sandwich slab is another type that is being widely used in marine and aerospace structures (Gibson and Ashby 1997; Kalamkarov and Polpakov 1997; Parton and Kudryavtsev 1993; Noor et al. 1996; Meguid and Kalamkarov 1994).

A possible method of analysis of cast-in-place hollow-core

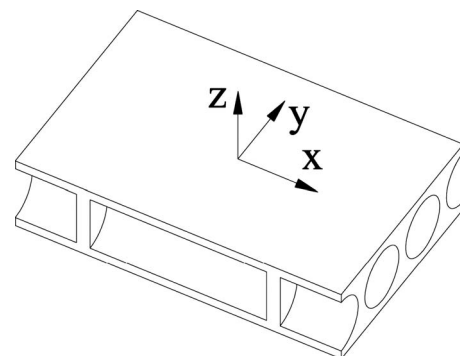


Fig. 1. Cylindrical hollow-core slab

¹Lecturer, Dept. of Civil Engineering, Shanghai Jiaotong Univ., Huashan Rd. 1954, Shanghai 200030, People's Republic of China (corresponding author). E-mail: xiejz@sjtu.edu.cn

Note. This manuscript was submitted on July 25, 2006; approved on May 11, 2009; published online on August 14, 2009. Discussion period open until February 1, 2010; separate discussions must be submitted for individual papers. This paper is part of the *Journal of Structural Engineering*, Vol. 135, No. 9, September 1, 2009. ©ASCE, ISSN 0733-9445/2009/9-1040-1047/\$25.00.

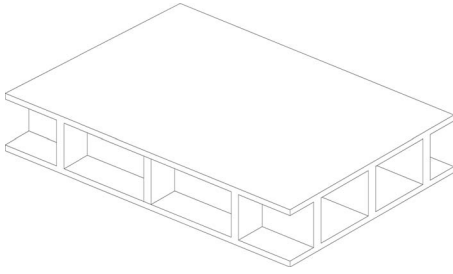


Fig. 2. Cubic hollow-core slab

slab is to treat the slab as a homogenous uniform continuum with an equivalent bending and shear stiffness. Unlike a method that is often used to account for precast hollow-core slabs which may be treated as a uniaxial member, the cast-in-place hollow-core slab is subjected to biaxial loading and it is an orthogonal anisotropic elastic continuum.

The macroscopic constitutive relationships of the cast-in-place hollow-core slab, especially at the transverse section of the cylindrical hollow-core slab, have seldom been researched according to available literature (Young and Budynas 2002). Though the Poisson's ratio is generally involved in the formulas of equivalent elastic moduli for honeycomb-core slab (Gibson and Ashby 1997; Kalamkarov and Polpakov 1997; Parton and Kudryavtsev 1993), the value of Poisson's ratio itself and the relevant computing method are seldom addressed.

In this paper, a formula derived analytically is proposed for computing a macroscopic Poisson's ratio. In addition, formulas for equivalent Young's modulus and shear elastic modulus are proposed for the transverse section of a cylindrical hollow-core slab. Moreover, a transverse rib effect which results in an increase in stiffness is also revealed.

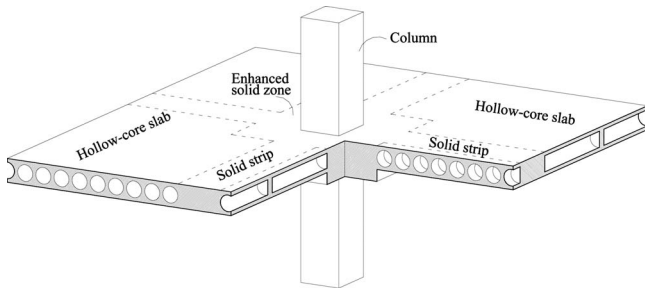


Fig. 3. Hollow-core slab in slab-column structures



Fig. 4. Cast-in-place hollow-core slab in practical engineering

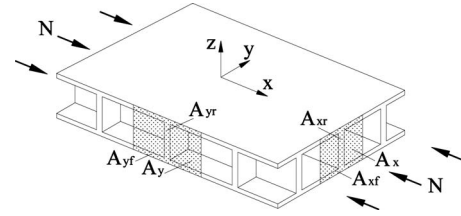


Fig. 5. Cubic hollow-core slab under uniform compression

Microscopic Poisson's Ratio

The Poisson's ratio is the ratio of transverse strain to longitudinal strain under uniaxial uniform compression or tension. Therefore, the macroscopic Poisson's ratio for a hollow-core slab can be obtained by applying axial uniform compression in plane.

As a relatively simple case, the cubic hollow-core slab is considered first. In the usual cast-in-place cubic hollow-core slab, as shown in Fig. 2, the thickness of the rib is usually about 0.1 m while the distance between the ribs is about 1.0 m. The thickness is therefore relatively small compared to the distance. Therefore, some assumptions can be adopted:

1. The influence of the rib thickness can be neglected, including the possible stress fluctuation in the face sheets.
2. The stress in the inner rib will be assumed to be uniformly distributed.

Derivation of Poisson's Ratio μ and the Transverse Rib Effect

For the cubic hollow-core slab as shown in Fig. 5, the longitudinal rib is along the direction of compressive force, and the other is the transverse rib. Neglecting the transverse, the biaxial rib slab becomes a uniaxial rib slab, as shown in Fig. 6. In this case, the longitudinal rib and the outer face sheets can freely deform without any constraint, thus it can be concluded that its lateral deformation is equal to that of the homogenous slab (to be ascertained by following numerical evaluation). The Poisson's ratio for the uniaxial rib slab in the longitudinal direction is the same as the μ_0 of the fundamental material. Therefore, the initial longitudinal strain ϵ_{x0} and transverse strain ϵ_{y1} can be obtained

$$\epsilon_{x0} = \frac{N}{(A_{yf} + A_{xr})E_0} \quad (1)$$

$$\epsilon_{y1} = \mu_0 \epsilon_{x0} \quad (2)$$

where E_0 = Young's modulus of the fundamental material; A_{xr} = sectional area of longitudinal rib; and A_{yf} = sectional area of relevant face sheets between two longitudinal ribs (see Fig. 5).

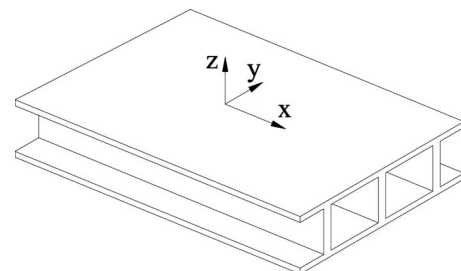


Fig. 6. Relevant uniaxial rib slab

When transverse ribs are present, displacement compatibility requires the strain in the transverse rib to be equal to the transverse strain of the slab. Accordingly, an additional tensile axial force exists in the transverse rib, i.e.

$$N'_y = \varepsilon_{y1} A_{yr} E_0 \quad (3)$$

Because the transverse rib does not directly carry an external force, its strain is caused by the restraint action that comes from the face sheets. To satisfy the equilibrium condition, N'_y should be reversely applied on lateral edge of the slab. Therefore, there is a transverse compressive strain

$$\varepsilon_{y2} = \frac{N'_y}{(A_{yf} + A_{yr})E_0} = \mu_0 \varepsilon_{x0} \gamma_y \quad (4)$$

$$\gamma_y = \frac{A_{yr}}{A_{yf} + A_{yr}} \quad (5)$$

where γ_y = ratio of transverse rib area to valid sectional area of the hollow-core slab.

The actual transverse strain is the difference between ε_{y1} and ε_{y2}

$$\varepsilon_y = \varepsilon_{y1} - \varepsilon_{y2} = \mu_0 \varepsilon_{x0} (1 - \gamma_y) \quad (6)$$

Meanwhile, the lateral force N'_y also results in an additional longitudinal strain in the slab. Similar to Eqs. (5) and (6), the strain can be directly obtained as follows:

$$\varepsilon'_x = \mu_0 \varepsilon_{y2} (1 - \gamma_x) = \mu_0^2 \varepsilon_{x0} \gamma_y (1 - \gamma_x) \quad (7)$$

$$\gamma_x = \frac{A_{xr}}{A_{xf} + A_{xr}} \quad (8)$$

Thus, the final longitudinal strain in the slab is the difference between ε_{x0} and ε'_x , i.e.

$$\varepsilon_x = \varepsilon_{x0} - \varepsilon'_x = \frac{N}{(A_{xf} + A_{xr})E_0} [1 - \mu_0^2 \gamma_y (1 - \gamma_x)] \quad (9)$$

Of course, the additional longitudinal strain ε'_x will lead to further additional reverse strain. However, considering Eq. (7), it can be seen that this kind of strain is very small and can be neglected.

According to Eq. (9), because of the influence of the transverse rib, the macroscopic equivalent elastic modulus of a biaxial rib slab is

$$E'_x = \frac{E_0}{1 - \mu_0^2 \gamma_y (1 - \gamma_x)} \quad (10)$$

Apparently, there is always $E'_x > E_0$. This phenomenon, in which the restraint of the transverse rib results in an increase in the macroscopic elastic modulus of a biaxial rib slab, is named as transverse rib effect in this paper.

Furthermore, the elastic modulus of the macroscopically equivalent homogenous slab can be expressed as

$$E_x = \frac{E_0 \lambda_x}{1 - \mu_0^2 \gamma_y (1 - \gamma_x)} \quad (11)$$

where

$$\lambda_x = (A_{xf} + A_{xr})/A_x \quad (12)$$

According to Eqs. (6) and (9), there is

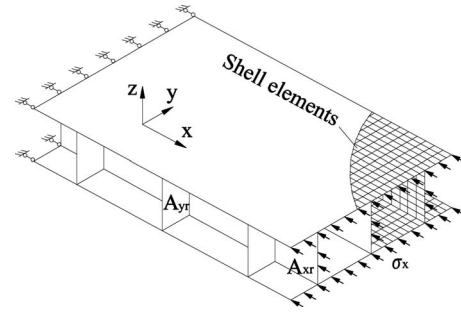


Fig. 7. FEM model

$$\mu_x = \frac{\varepsilon_y}{\varepsilon_x} = \mu_0 \frac{1 - \gamma_y}{1 - \mu_0^2 \gamma_y (1 - \gamma_x)} \quad (13)$$

In the above equation, the numerator is always smaller than the denominator. Therefore, it can be concluded that the macroscopic Poisson's ratio of the hollow-core slab is always smaller than μ_0 of the fundamental material.

Theoretical Verification

There is the identical equation for the orthogonal anisotropic elastic plane

$$\mu_x/E_x = \mu_y/E_y \quad (14)$$

Let us verify whether the proposed formulas satisfy this identical equation. Using Eqs. (11) and (13), we can obtain

$$\frac{\mu_x}{E_x} = \frac{\mu_0}{E_0} \frac{1 - \gamma_y}{\lambda_x} = \frac{\mu_0}{E_0} \frac{A_{yf} A_x}{(A_{yf} + A_{yr})(A_{xf} + A_{xr})} \quad (15)$$

Noticing all the sectional areas in above expression are relative values, there is $A_{xf} = A_{yf}$ when $A_x = A_y$ so that the right portion of the expression is irrelevant to the directions, and the proposed formulations in this paper naturally satisfies the identical Eq. (14).

Numerical Verification

The proposed formulas are to be verified by numerical examples. The cubic hollow-core slab with total thickness of 0.6 m is chosen as the examples. The distances between ribs in both directions are 1.2 m, and thickness of the face sheets is 0.1 m. Let thickness of the longitudinal rib be 0.1 m and keep it invariable, and let thickness of the transverse rib vary from 0.0m to 0.3 m; the geometrical parameters of the slab are $A_{xf} = 0.24 \text{ m}^2$, $A_{yr} = 0.03 \sim 0.18 \text{ m}^2$, $\gamma_y = 1/9 \sim 3/7$, $\lambda_y = 3/8 \sim 7/12$, and $\mu_0 = 0.25$ and $E_0 = 1000 \text{ MPa}$ for fundamental material.

The commercial program ANSYS is employed here for computation. Both the ribs and the face sheets are subdivided into the Shell-63 element of ANSYS. The finite-element method (FEM) model is shown in Fig. 7. An axial compressive force $\sigma_x = 0.1 \text{ MPa}$ is uniformly applied on the ribs and face sheets in longitudinal direction (the x-direction in Fig. 7). Only the displacement opposite to the force and rigid body displacements are constrained. The results are shown in Table 1.

When the thickness of transverse rib is 0, the cubic hollow-core slab becomes a uniaxial rib slab. Its Poisson's ratio, as shown in Table 1, is still the value of the fundamental material. This verifies the conclusion about the uniaxial rib slab as previously described.

Table 1. Poisson's Ratio and Elastic Modulus of Cubic Hollow-Core Slab

Thickness of transverse rib (<i>m</i>)	Numerical results				Proposed results	
	Longitudinal strain $\varepsilon_x \times 10^{-3}$	Transverse strain $\varepsilon_y \times 10^{-3}$	Poisson's ratio μ_x	Elastic modulus E'_x/E_0	Poisson's ratio μ_x	Elastic modulus E'_x/E_0
0.0	100.0	25.0	0.25	1.0	0.25	1.0
0.05	99.3161	21.8047	0.2195	1.0069	0.2235	1.0056
0.10	98.8458	19.4109	0.1964	1.0101	0.2020	1.0101
0.15	98.4825	17.5163	0.1779	1.0154	0.1843	1.0138
0.20	98.2071	15.9712	0.1626	1.0183	0.1695	1.0169
0.25	97.9736	14.6830	0.1499	1.0207	0.1569	1.0196
0.30	97.7776	13.5906	0.1390	1.0227	0.1460	1.0219

Table 1 shows that the longitudinal Poisson's ratio μ_x is always smaller than the μ_0 of the fundamental material, and the values of the μ_x decrease gradually as the transverse rib increases in thickness. This characteristic is reflected with both the numerical results and proposed theoretical results. Moreover, the difference between numerical and theoretical results is small, which illustrates that the adopted assumptions and obtained formulas are reasonable.

It can also be found from Table 1 that the longitudinal strains ε_x with transverse rib are smaller than that without transverse rib, which proves that the transverse rib effect actually exists. The phenomenon becomes more apparent as the sectional area of transverse rib increases.

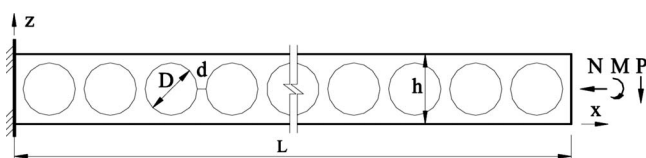
Treatment for Cylindrical Hollow-Core Slab

For the cylindrical hollow-core slab, as shown in Fig. 1, the longitudinal rib (parallel to the inner tube) has high and variable thickness, which does not satisfy the two assumptions in the analysis. However, the transverse rib is thin and uniform, which agrees with the assumptions. Therefore, the Poisson's ratio and elastic modulus along the inner tube can be directly computed with Eqs. (11) and (13). The Poisson's ratio transverse to the inner tube can be indirectly obtained by the identical Eq. (14) after obtaining relevant transverse elastic moduli, which will be introduced in the following section.

Macroscopic Young's Moduli

There are two aspects for macroscopic Young's moduli with different values, the bending modulus and axial compression modulus. The macroscopic equivalent elastic moduli should be computed according to the geometrical characters of the hollow-core slabs, and the computational methods are different for cylindrical and cubic hollow-core slab.

For the cubic hollow-core slab, as previously described, the thickness of the rib is relatively small in comparison to the distances between ribs. Therefore, the macroscopic elastic moduli

**Fig. 8.** Cross section of cylindrical hollow-core slab

can be computed based on one-way rib and face sheets, and then increased considering the transverse rib effect as described in Eq. (10).

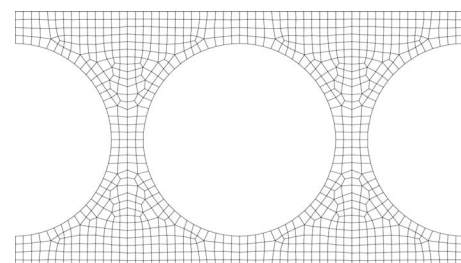
For the cylindrical hollow-core slab, different computing methods should be respectively adopted in two orthogonal directions because of their different sectional configurations. The macroscopic elastic modulus along the inner tube, whose transverse rib is similar to that of the cubic hollow-core slab, can be treated in the same way as for the cubic hollow-core slab. The moduli in the direction vertical to the inner tube should be computed by considering the influence of rib of nonuniform thickness.

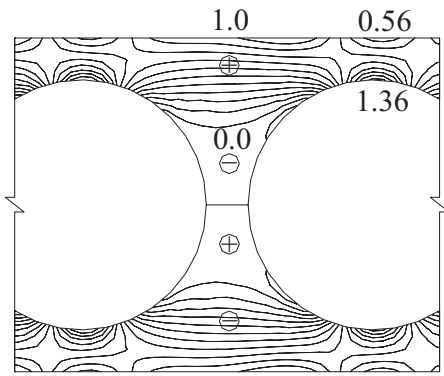
The cross section of the cylindrical hollow-core slab without the transverse rib is shown in Fig. 8. The stiffness for this kind of beam with longitudinally distributed large hole has seldom been studied. Analogous configurations can be found in steel beam in which large holes decrease member weight and slow down heat transport. However, the stiffness of the steel beam mainly comes from its flanges, and the stiffness of this kind of web with large holes is usually neglected. The treatment is not appropriate for the cylindrical hollow-core slab. A direct analytical solution for this beam type is very difficult and we should rely on numerical approach.

Stress Analysis

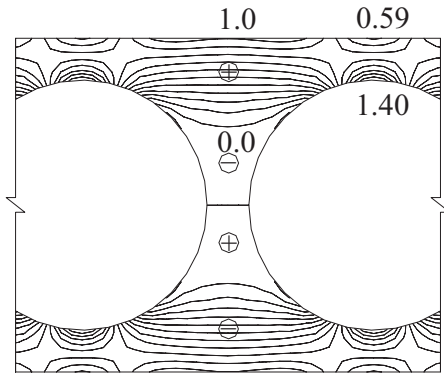
The FEM is employed here to analyze the mechanical characteristics of cylindrical hollow-core slab on transverse cross section. The subdivided mesh of FEM is shown in Fig. 9. The obtained stress distributions for bending shear, pure bending, and axial force are shown in Fig. 10, in which the normalized stress values are indicated with unit value at the edge opposite to the rib.

It can be found from these figures that the stresses vary significantly over the cross section. At the narrowest strip opposite to the inner hole, the stress at the outer edge is less than 1.0, and the stress at the inner edge exceeds 1.0. There are explicit zero-stress

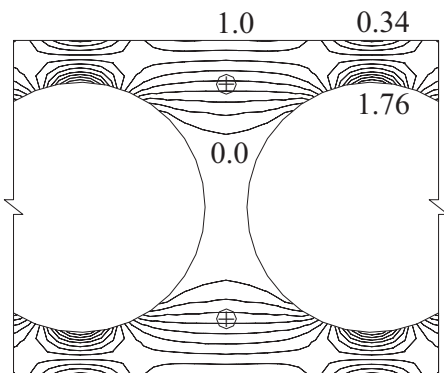
**Fig. 9.** Subdivided FEM mesh



(a) Bending and shear



(b) Pure bending



(c) Axial force

Fig. 10. Distributions of horizontal stresses σ_x over cross section of the cylindrical hollow-core slab

curves at the half height of the rib of variable thickness, and the stresses inside the curves are very small. These are common characteristics.

The observation that the medium portion of the rib is the zero-stress zone indicates that this portion contributes nothing to the bending and axial stiffness and can be neglected while computing macroscopic equivalent elastic modulus. Moreover, in the macroscopic homogenization process, the microscopic fluctuation of the stress can also be neglected. We can obtain the macroscopic equivalent bending and axial elastic modulus by selecting an effective cross-sectional area.

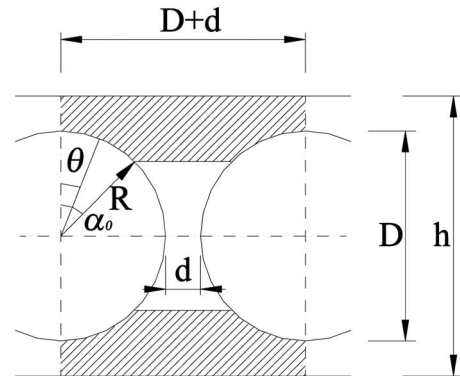


Fig. 11. Effective area of transverse section

Equivalent Models

Assume the zero-stress curve to be a straight line, and denote the vertical slope angle of the radius corresponding to that line as α_0 , as shown in Fig. 11, and we can obtain the integrating sum ψ_I of the bending inertia $I(x)$ at a periodic segment $(D+d)$, i.e.

$$\psi_I = \int_0^{D+d} I(x) dx = \frac{1}{12} b h^3 [\eta_1 D \sin \alpha_0 + \eta_2 (d + D - D \sin \alpha_0)]$$

where

$$\eta_1 = 1 - \frac{D^3}{h^3 \sin \alpha_0} \left(\frac{3}{8} \alpha_0 + \frac{1}{4} \sin 2\alpha_0 + \frac{1}{32} \sin 4\alpha_0 \right)$$

$$\eta_2 = 1 - \frac{D^3}{h^3} \cos^3 \alpha_0 \quad (16)$$

and b = thickness which can be treated as 1.

In the course of homogenization, the thickness of the slab is invariable, what really changes is the elastic modulus. Using the value ψ_I , the macroscopic bending modulus E_M for transverse section of cylindrical hollow-core slab can be directly obtained

$$E_M = E_0 \frac{\eta_1 D \sin \alpha_0 + \eta_2 (d + D - D \sin \alpha_0)}{D + d} \quad (17)$$

Similarly, using the integrating sum ψ_A of effective sectional area at a periodic segment $D+d$

$$\psi_A = \int_0^{D+d} A(x) dx = b h D (\eta_3 + \eta_4)$$

where

$$\eta_3 = \sin \alpha_0 - \frac{D}{2h} \left(\alpha_0 + \frac{1}{2} \sin 2\alpha_0 \right)$$

$$\eta_4 = \left(\frac{d}{D} + 1 - \sin \alpha_0 \right) \left(1 - \frac{D}{h} \cos \alpha_0 \right) \quad (18)$$

The macroscopic axial compression modulus E_N can also be obtained

$$E_N = E_0 \frac{D(\eta_3 + \eta_4)}{D + d} \quad (19)$$

Finally, the unknown parameter α_0 in Eqs. (17) and (19) is to be resolved by numerical means of the subdivided FEM model. A large number of numerical solutions show that the values of α_0 are mainly the same under all bending shear, pure bending, and

Table 2. Equivalent Macroscopic Elastic Modulus of Cylindrical Hollow-Core Slab at Transverse Section

Load case	Model	Displacement of uniform beam (theoretical) (mm)	Results of FEM			Proposed methods E_M/E_0 or E_N/E_0
			Displacement of uniform beam (mm)	Displacement of hollow-core (mm)	E_M/E_0 or E_N/E_0	
<i>M</i>	I	4.332	4.332	7.589	0.571	0.572
	II	8.461	8.461	1.289	0.656	0.648
	III	8.820	8.820	11.442	0.771	0.754
<i>N</i>	I	1.900×10^{-2}	1.900×10^{-2}	7.728×10^{-5}	0.246	0.241
	II	2.375×10^{-1}	2.375×10^{-1}	7.930×10^{-4}	0.299	0.284
	III	2.100×10^{-2}	2.100×10^{-2}	5.414×10^{-5}	0.388	0.348

axial force actions. To facilitate practical usage, a simplified and uniform value is suggested here for the most usual cases of the cylindrical hollow-core slab as

$$\alpha_0 = \pi/8 \quad (20)$$

Numerical Verification

Three usual cylindrical hollow-core slabs are selected as the numerical examples. A unit width slab with large holes is computed as a cantilever beam under some tip loads (see Fig. 11). The geometrical parameters of the cantilever beams are:

1. $h=0.5$ m, $D=0.4$ m, $d=0.05$ m, and $L=9.5$ m;
2. $h=0.4$ m, $D=0.3$ m, $d=0.05$ m, and $L=9.5$ m; and
3. $h=0.3$ m, $D=0.2$ m, $d=0.05$ m, and $L=6.3$ m.

Where the meaning of L , h , D , and d can be found in Fig. 11. The commercial program ANSYS is still used here and the subdivided mesh of the Shell-63 element in the ANSYS is shown in Fig. 8.

For comparison, three uniform beams with the same material and sections are also computed. The tip displacement ratio of the circular hole beam to that of uniform beam reflects the relationship between the macroscopic elastic modulus E_M/E_N and fundamental E_0 . For the uniform beams, both numerical and theoretical solutions can be obtained for verification.

Under the loads $M=1.0$ kN m and $N=1.0$ kN acted on the tip of the beams, the tip displacements of the beams and other relevant results are shown in Table 2. The numerical results and the

theoretical displacement for the uniform beam are the same, which indicates the validity of the examples.

Table 2 shows that the macroscopic equivalent elastic moduli obtained with the proposed method are highly consistent with that of the numerical method. The valid sectional area method and the suggestion of $\alpha_0=22.5^\circ$ for the transverse section of the cylindrical hollow-core slab are verified to be reasonable and correct.

Macroscopic Shear Modulus of Cylindrical Hollow-Core Slab

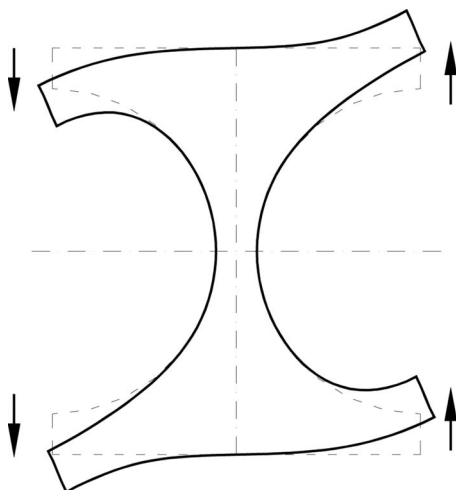
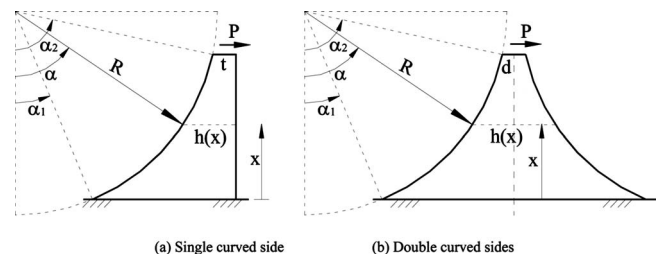
There have been many studies in the macroscopic shear modulus of honeycomb-core slab (Xu et al. 2001; Davalos et al. 2001; Shi and Tong 1995; Grediac 1993), in which the rib was thin walled and its stress was treated as uniform distribution. However, to the transverse section of cylindrical hollow-core slab, which is a kind of elastic continuum with large holes (see Fig. 11), the assumption of the uniform stress distribution is not reasonable.

Equivalent Models

A typical shear deformation shape of the cylindrical hollow-core slab in the transverse direction is shown in Fig. 12. It can be found that the shear deformation of the slab can be considered as a combination of bending-shear deformations of its rib and face sheets of variable thickness. Thus, the equivalent shear modulus can be obtained by computing the bending-shear deformation of the rib and face sheets in a periodic segment.

The rib and face sheets of the cylindrical hollow-core slab are special beams with curved sides, and relevant displacement formulas are not available in the existing literature, so the bending-shear displacement formulas for cantilever beam with curved sides are deduced first.

The cantilever beams with curved sides are shown in Fig. 13. The length of the beams is denoted by the arc angle α_1 and α_2 of

**Fig. 12.** Shear deformation at a periodic segment**Fig. 13.** Beam with curved sides

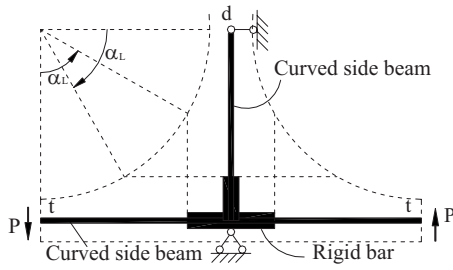


Fig. 14. Equivalent shear model for transverse section of hollow-core slab

the curved sides. The beam with single curved side is the case of the face sheet and the beam with double curved sides is the case of the rib of variable thickness, respectively.

For the single curved side beam in Fig. 13(a), neglecting the offset of neutral axis, the tip displacements of the beam under a concentrated shear force $P=1$ is

$$\begin{aligned} \delta_{\text{arc}1} &= \delta_{\text{arc}M} + \delta_{\text{arc}Q} \\ \delta_{\text{arc}M} &= \frac{12}{bE_0} \left[(\alpha_2 - \alpha_1) + \varphi(\cos \alpha_2 - \cos \alpha_1) \right. \\ &\quad \times \frac{(R+t) - 2(1 - \varphi \sin \alpha_1)}{2(1 - \varphi \sin \alpha_1)^2} \\ &\quad + \frac{3\varphi^2 - 2}{\sqrt{1 - \varphi^2}} \left(\text{arctg} \frac{\xi_2 - \varphi}{\sqrt{1 - \varphi^2}} - \text{arctg} \frac{\xi_1 - \varphi}{\sqrt{1 - \varphi^2}} \right) \\ &\quad \left. + \frac{\varphi}{1 - \varphi^2} \left(\frac{\varphi \xi_2 - 1}{\xi_2^2 + 2\varphi \xi_2 + 1} - \frac{\varphi \xi_1 - 1}{\xi_1^2 + 2\varphi \xi_1 + 1} \right) \right] \delta_{\text{arc}Q} \\ &= \frac{1}{bG_0} \left[\frac{2}{\sqrt{1 - \varphi^2}} \left(\text{arctg} \frac{\xi_2 - \varphi}{\sqrt{1 - \varphi^2}} - \text{arctg} \frac{\xi_1 - \varphi}{\sqrt{1 - \varphi^2}} \right) \right. \\ &\quad \left. - (\alpha_2 - \alpha_1) \right] \end{aligned} \quad (21)$$

$$\varphi = R/(R+t), \quad \xi_1 = tg(\alpha_1/2), \quad \xi_2 = tg(\alpha_2/2) \quad (21)$$

where $\delta_{\text{arc}M}$ =bending deformation; $\delta_{\text{arc}Q}$ =shear deformation; and b =thickness of the beam which can be treated as 1.

Eq. (21) is also fit for the double curved sides beam in Fig. 13(b). Substitute $t=d/2$ into Eq. (21), and the final tip displacement is

$$\delta_{\text{arc}2} = \frac{1}{8} \delta_{\text{arc}M} + \frac{1}{2} \delta_{\text{arc}Q} \quad (22)$$

Using Eqs. (21) and (22), the shear deformation of cylindrical hollow-core slab in the transverse direction can be computed. As shown in Fig. 14, the rib with variable thickness is treated as a single curved side beam [see Fig. 13(b)] and face sheets as double curved sides beam [see Fig. 13(a)]. The length of the beams are determined by the arc angle α_L , and the beams are connected by rigid bars in the core zone. The arc angles α_1 and α_2 in Fig. 13 are expressed with α_L as

$$\alpha_1 = \pi/2 - \alpha_L, \quad \alpha_2 = \pi/2$$

Substitute the values α_1 and α_2 in Eqs. (21) and (22) to obtain the tip displacements of curved side beams. Therefore, the entire shear deformation of the section in Fig. 14 under shear force P can be obtained. Finally, we obtain the expression of the equivalent shear modulus of cylindrical hollow-core slab in transverse direction as

$$G_Q = \frac{1}{(R+t) \left(\frac{2\delta_{\text{arc}1}}{2R+d} + \frac{4\delta_{\text{arc}2}}{2R+t} \right)} \quad (23)$$

Though the analytical solutions of Eqs. (21) and (22) are used in this case, it should be considered that this model is still a practical method because treating ribs and face sheets with variable thickness as curved side beams is actually a simplification, which provides a relatively accurate and easy method for practical utilization. Therefore, the value of the angle α_L needs to be determined by FEM solution. Comparing with the results of the FEM, α_L can be set as

$$\alpha_L = \pi/2 \quad (24)$$

Numerical Verification

Because pure shearing state is difficult to simulate, we seek indirect means to verify the equivalent shear modulus. In the above section, the long cantilever beams have been chosen in verifying the proposed macroscopic Young's moduli, in which the shear displacement is small and can be neglected. Therefore, we can use the same models (Figs. 8 and 11) here with a shorter length in which the shear displacement becomes significant. The macroscopic Young's moduli in Table 2 are also used here for computing the theoretical bending displacement, and those obtained by FEM are selected to avoid possible systematic error.

The relevant macroscopic moduli for the examples are:

1. $E_M/E_0=0.571$ and $G_Q/G_0=0.0258$ 8;
2. $E_M/E_0=0.656$ and $G_Q/G_0=0.0382$ 1; and
3. $E_M/E_0=0.771$ and $G_Q/G_0=0.06423$.

Under the vertical shear force $P=10$ kN acting at the tip of the beams, the results of FEM with the mesh shown in Fig. 8 and the

Table 3. Tip Displacement of Short Cantilever Beam with Cylindrical Hollow-Core (Unit: Millimeter)

Length of the beam	Model I		Model II		Model III	
	Displacement of FEM	Proposed (shear part)	Displacement of FEM	Proposed (shear part)	Displacement of FEM	Proposed (shear part)
$(D+d) \times 2$	2.152	2.078 (1.670)	1.525	1.426 (1.099)	0.853	0.863 (0.623)
$(D+d) \times 3$	3.971	3.881 (2.505)	2.835	2.752 (1.649)	1.703	1.745 (0.934)
$(D+d) \times 4$	6.710	6.603 (3.340)	4.878	4.813 (2.198)	3.093	3.164 (1.246)
$(D+d) \times 5$	10.673	10.547 (4.175)	7.900	7.854 (2.748)	5.204	5.310 (1.557)
$(D+d) \times 6$	16.169	16.021 (5.010)	12.146	12.121 (3.298)	8.215	8.353 (1.868)

results of the mechanical solution with proposed macroscopic modulus G_Q in Eq. (23) are shown in Table 3. They are highly consistent.

Conclusions

1. The formulas for computing Poisson's ratio of cast-in-place hollow-core slabs with bilateral ribs are deduced by theoretical means at first. For the cubic hollow-core slab, the Poisson's ratios in two orthogonal directions can be directly computed with the proposed formulas. For the cylindrical hollow-core slab, the Poisson's ratio along the inner tube can be directly computed with the formulas, and the Poisson's ratio in the other direction can be indirectly obtained by the relationship between elastic modulus and Poisson's ratios in two orthogonal directions.
2. In the course of deducing the formulas for Poisson's ratio, the so-called transverse rib effect, in which the transverse rib may lead to stiffness increase in the slab, is also shown. The numerical examples illustrate this phenomenon.
3. Based on the stress distribution characteristic revealed by numerical results of FEM, an effective sectional area method is advocated in computing macroscopic elastic moduli of cylindrical hollow-core slab in the transverse direction. The effective section consists of the outer portions of the transverse section with a straight boundary, which is suggested at a radial distance with a vertical angle $\alpha_0=22.5^\circ$.
4. The shear deformation of cylindrical hollow-core slab in the transverse direction is the combination of bending-shear deformations of the rib and face sheets of variable thickness. With the newly deduced formulas of the curved sides beam, the equivalent shear modulus is proposed by solving the equivalent frame which consists of the curved sides beams and inner rigid bars.
5. All the proposed methods and formulas are verified by theoretical or numerical means.

Notation

The following symbols are used in this paper:

- A_x, A_{xr}, A_{xf} = gross cross-sectional areas of hollow-core slab, cross area of rib and face sheet in x -direction;
- A_y, A_{yr}, A_{yf} = gross cross areas of hollow-core slab, cross area of rib and face sheet in y -direction;
- b = thickness of cross section of cantilever beam;
- d = minimum thickness of rib in cylindrical hollow-core slab;
- D, R = diameter and radius of inner cylindrical mold;
- E_0, G_0 = Young's modulus and shear modulus of fundamental material;
- E_M, E_N = equivalent Young's modulus under bending moment and axial force for cylindrical hollow-core slab in transverse direction;
- E_x, E_y = equivalent Young's modulus under axial force in x - and y -directions;

- G_Q = equivalent shear modulus for cylindrical hollow-core slab in transverse direction;
- h = total thickness of hollow-core slab and height of cross section of cantilever beam;
- $I(x)$ = bending inertia;
- N, M, P = axial force, bending moment, and shear force;
- t = minimum thickness of varied face sheet in cylindrical hollow-core slab;
- γ_x, γ_y = area ratio of rib section to net section of hollow-core slab in x - and y -directions;
- $\delta_{\text{arc}1}, \delta_{\text{arc}2}$ = total tip displacement of cantilever beam with single curved side and double curved sides;
- $\delta_{\text{arc}M}, \delta_{\text{arc}Q}$ = tip displacement of cantilever curved sides beam caused by pure bending moment and shear force;
- λ_x, λ_y = area ratio of net cross section to gross cross section of hollow-core slab in x - and y -directions;
- μ_0 = Poisson's ratio of fundamental material; and
- μ_x, μ_y = macroscopic Poisson's ratio in x - and y -directions.

References

- China Association for Engineering Construction Standardization (CECS). (2004). "Technical specification for cast-in-place concrete hollow floor structures." *CECS 175-2004*, China Planning, Beijing.
- Davalos, J. F., Qiao, P., Xu, X. F., Robinson, J., and Barth, K. E. (2001). "Modeling and characterization of fiber-reinforced plastic honeycomb sandwich panels for highway bridge applications." *Compos. Struct.*, 52(3-4), 441-452.
- DIN. (1988). "Beton und Stahlbeton" *DIN 1045*, Beuth Verlag, Berlin (in German).
- Gibson, L. J., and Ashby, M. F. (1997). *Cellular solids: Structure and properties*, Cambridge University Press, Cambridge, Mass.
- Grediac, M. (1993). "A finite element study of the transverse shear in honeycomb cores." *Int. J. Solids Struct.*, 30(13), 1777-1788.
- Huang, Y., Ma, K. J., Zhang, H. G., and Xiao, J. C. (1997). "Study and application of viereendeel-sandwich-plate floor framing in multistoried and tall buildings." *J. Building Structures*, 18(6), 55-64 (in Chinese).
- Kalamkarov, A. L., and Polpakov, A. G. (1997). *Analysis, design, and optimization of composite structures*, Wiley, New York.
- Lou, W. J., Wu, X. P., Chen, Y., Lu, D., Cai, Y. T., and Lu, S. L. (2005). "Full scale experimental study of prestressed concrete hollow cast floor slab." *J. Zhejiang Univ. Sci.*, 39(8), 1223-1228.
- Meguid, S. A., and Kalamkarov, A. L. (1994). "Asymptotic homogenization of elastic composite materials with a regular structure." *Int. J. Solids Struct.*, 31(3), 303-316.
- Noor, A., Burton, W. S., and Bert, C. W. (1996). "Computational models for sandwich panels and shells." *Appl. Mech. Rev.*, 49(3), 155-199.
- Parton, V. Z., and Kudryavtsev, B. A. (1993). *Engineering mechanics of composite structures*, CRC, Boca Raton, Fla.
- Schnellenbach-Held, M., and Pfeffer, K. (2002). "Punching behavior of biaxial hollow slabs." *Cem. Concr. Compos.*, 24(6), 551-556.
- Shi, G., and Tong, P. (1995). "Equivalent transverse shear stiffness of honeycomb cores." *Int. J. Solids Struct.*, 32(10), 1383-1393.
- Xu, X. F., Qiao, P., and Davalos, J. F. (2001). "Transverse shear stiffness of composite honeycomb core with general configuration." *J. Eng. Mech.*, 127(11), 1144-1151.
- Young, W. C., and Budynas, R. G. (2002). *Roark's formulas for stress and strain*, 7th Ed., McGraw-Hill, New York.